Anomalous phase behavior of liquid–vapor phase transition in binary mixtures of DNA-coated particles

Francisco J. Martinez-Veracoechea,*[a] Behnaz Bozorgui[b] and Daan Frenkel[a]

Received 23rd June 2010, Accepted 21st September 2010
DOI: 10.1039/c0sm00567c

We report a Monte Carlo study of a 1 : 1 binary mixture of particles coated with DNA chains with "sticky" ends. The system was modeled using a coarse-grained representation. In order to map out the phase diagram of this model system we combined biased Monte Carlo simulations with histogram reweighting techniques. We find that, at low temperatures (strong hybridization) this system undergoes a phase separation between a dilute vapor-like phase and a dense network-forming liquid-like phase. We observe a surprising non-monotonic dependence of the coexistence pressure on the temperature, or more precisely, on the reduced hybridization free energy (f_{hyb}/k_BT). This anomalous behavior can be understood in terms of a cross-over between two distinct regimes for the driving force of the phase transition: a hybridization-free-energy-driven regime and an entropy-driven regime. In the former regime, we observe a "normal" vapor–liquid equilibrium where during condensation, the system gains hybridization free energy but loses entropy. In the entropy-driven regime, the phase transition is driven by the increase in entropy due to the re-arrangement of sticky-end bonds in the liquid phase. Finally, we observe that the system can only undergo phase separation if the valence (*i.e.*, the number of DNA-chains per particle) is larger than two. The coexistence region widens markedly as the valence is increased.

Introduction

The interesting feature of colloidal systems coated with DNA chains is that the specificity of Watson–Crick type interactions can in principle be exploited to control the self-assembly of complex colloidal structures.[1–3] In one possible implementation, the DNA molecules are chemically grafted to the colloidal surface at one end, while having a single-stranded "sticky" end on the other side of chain.[4] Moreover, the single-stranded end can be designed to hybridize specifically and reversibly with a complementary single-stranded DNA (ssDNA) sequence that presents the "correct" (*i.e.*, complementary in the Watson–Crick sense) nucleotide sequence (see, however, ref.5 for a description of the relevance of non-Watson–Crick interactions). An alternative strategy is based on the use of dissolved, free DNA "linkers" with sticky ends that can bind simultaneously to the (shorter) complementary ssDNA sequences that are bound to the surface of two colloids.[1] These general strategies have been used successfully to drive the assembly of both FCC and BCC crystals of gold nanoparticles.[6–11] In addition, the lattice constants of the crystals thus formed can be controlled through the design of the DNA chains that bind the colloids together.[12] While nano-colloids coated with short DNA strands can form crystals with relative ease, this is not the case for larger colloids coated with long DNA. In that case, the system either forms finite clusters or a disordered percolating network.[4,13]

Despite the substantial amount of progress that has been made, the self-assembling capabilities of these DNA-guided systems have yet to reach their full potential. The wide morphological diversity of crystals theoretically predicted by Tkachenko[14] is yet to be observed. And more importantly, applications where the DNA-coated particles can be assembled in a controlled manner, in nano-blocks of specific geometries, remain a challenge.[15–17]

In order to effectively uncover the full potential of these general class of DNA-driven systems it is mandatory to gain a better understanding of their underlying phase behavior. Although progress has been made in improving the understanding of the role of the DNA-chain configurational entropy in the binding process,[18,19] a complete understanding of the thermodynamics behind the self-assembly of these complex systems is still lacking.

Molecular simulations provide a convenient way of exploring, in a well-defined environment, the large parameter space of this class of systems, while giving valuable insight about the underlying physics. Thus, not surprisingly, much simulation work has been devoted to the study of DNA-coated particles.[20–23] For example Molecular Dynamics simulations of a single DNA-coated gold nanoparticle have been carried out at the atomistic level to study the interaction between the DNA-chains and salt.[24] In addition, several studies have been made to develop suitable models for DNA chains.[25,26] However, a fully atomistic treatment of the DNA interactions becomes computationally prohibitive for the study of the phase behavior of many interacting colloids. It is therefore mandatory to make use of coarse-grained models. It is worth noting that coarse-grained models have been successfully used in the study of wide variety of polymeric and colloidal systems.[27–32] In the particular case of DNA-coated nanoparticles the Starr group[21,22] has carried out coarse-grained simulations in the regime where the DNA chains behave like rigid sticks and are much larger than the nanoparticle. This work revealed a variety of intriguing network phases.

[a]*Department of Chemistry, University of Cambridge, Lensfield Road, Cambridge, CB2 1EW, UK. E-mail: fjm45@cam.ac.uk*
[b]*Department of Chemistry, Columbia University, 3000 Broadway, New York, NY, 10027, USA*

Bozorgui and Frenkel[33] carried out Grand-Canonical (μVT) simulations of coarse-grained models for a binary mixture of colloids coated with long DNA strands, where the DNA of type-A colloids can only bind (through their sticky end) to the DNA of type-B colloids. The study of ref. 33 focused on the limit of infinitely strong hybridization (*i.e.*, there are no unbound "sticky" ends). Hence, in the very dilute limit this system is necessarily composed of A–B dimers where all the DNA chains are hybridized. As the chemical potential of the dimers was increased, this system was found to undergo a sudden transition to a dense, percolating phase. The transition showed marked hysteresis indicative of a first order phase transition. As there was no hybridization energy gain when forming the liquid phase (because both phases have all the bonds satisfied) the authors of ref. 33 concluded that the first order transition was entropy-driven, analogous to the one predicted on the basis of mean field theory by Zilmann *et al.*[34,35] for microemulsions with telechelic polymer linkers.

While the μVT Monte Carlo (MC) simulations used by Bozorgui and Frenkel,[33] were able to demonstrate the existence of a phase transition in the limit of infinite binding strength, this study could not determine the location of the thermodynamic coexistence curve nor, for that matter, could this study reveal how the transition varied with temperature (binding strength). To achieve this, more sophisticated simulation techniques such as Gibbs ensemble[36] MC or histogram reweighting[37] are needed.[38] Moreover, at high densities where the percolating-liquid phase forms, the equilibrium density of free dimers becomes vanishingly small. This makes dimer-deletion moves virtually impossible and, as a result, the chemical-potential equilibration in Gibbs-ensemble simulations becomes prohibitively slow.

In the present paper we develop a general MC methodology to study the condensation transition in systems of DNA-coated particles. The methodology circumvents the ergodicity problems associated with network formation thus allowing us to compute the free energy of the system.

In the following, we first present the coarse-grained model for DNA-coated particles. Then, we introduce the methodology for the prediction of liquid–vapor coexistence in this type of percolating system. We present results for the phase behavior of a 1 : 1 binary mixture of DNA coated particles as a function of the binding free energy and the number of DNA chains per colloid. In this study, the binding free energy plays a role analogous to that of temperature in conventional liquid–vapor phase diagrams. We also study in detail the causes of the anomalous phase behavior observed, showing that the non-monotonic dependence of the coexistence pressure on the binding free energy arises as a consequence of the crossover between "entropy-driven" and "hybridization-free-energy-driven" regimes of the phase transition. Finally, we show that coexistence region widens as the number of DNA-chains per particle is increased, suggesting that recent experiments with DNA-coated colloids[13] were likely performed inside the two-phase region.

Model

As in ref. 33 we use a minimalistic coarse-grained off-lattice model where colloids are represented as hard-spheres with a radius (R_c) equal to three times the DNA-chain radius of gyration (R_g). Each DNA chain is described by its center-of-mass position and interacts with other chains through an effective "soft blob" potential.[39] The effective blob–blob potential (V_{bb}) is

$$\beta V_{bb} = 1.75\exp\left[-0.80\left(r/R_g\right)^2\right] \quad (1)$$

where r is the distance between the centers of blobs, and $\beta = 1/k_bT$, with k_b Boltzmann's constant, and T the absolute temperature. From the work of refs 40 and 41 it is known that eqn (1) provides a good description of the interactions between polymer chains in a good solvent in the dilute regime. Eqn (1) provides a first order approximation of polymer-polymer interactions in our coarse grained model. The non-bonded interaction between a DNA chain and a hard colloid is approximated through:

$$\beta V_{cp} = A\exp\left[-B\left(r/R_g - C\right)\right] \quad (2)$$

with the values A = 3.1995, B = 4.1662, and C = 0.4996; chosen to reproduce the potential of mean-force between the center of mass of a self-avoiding walk (SAW) chain and a flat hard wall accurately up to $10k_bT$. Note, that for the colloid-polymer size ratio studied here (*i.e.*, $R_c/R_g = 3$) the effective interaction between the chain and the colloid is essentially the same as with a flat wall.[42]

Each DNA blob interacts with its anchoring point through,

$$\beta V_{tether} = \frac{3}{4}\left(\frac{r - R_c}{R_g}\right)^2 \quad (3)$$

where r is the distance between the center of the blob and the center of the colloid. Thus, effectively, the anchoring points are allowed to move relatively easily on the colloids' surface as it is the case on lipid vesicles coated with DNA[43] or gold nanoparticles with thiol bonds.[44] We expect that fixing the anchoring positions will not affect the qualitative conclusions of this paper, although the quantitative effects remain to be investigated.

It is essential to use a simple model for the DNA hybridization. Since the blobs represent relatively long DNA chains it is reasonable to assume that the length of the sticky end is much shorter than the rest of the chain. Therefore, when sticky ends of two different chains hybridize we should obtain a new single chain but with twice the length. In our coarse grained model we achieve this by simply taking the two original non-hybridized blobs and connecting them through a harmonic potential of the form:

$$\beta V_{har} = 0.534(r/R_g - 0.730)^2 \quad (4)$$

where r is the inter-blob distance, while keeping all the other interactions the same. Thus, effectively creating a new "longer" two-blob chain. Pierleoni *et al.*[41] have shown that if a SAW chain is divided in two blobs, each of them with a radius of gyration equal to R_g, a potential of the form of (4) can accurately describe the effective interactions between their centers of mass.

In the following all the distances will be measured in units of R_g, the energies in units of k_bT, and the pressures in units of k_bT/R_g^3.

Computationally, the prediction of the liquid–vapor coexistence curve of a system of colloids coated with long DNA is quite

challenging, because most conventional techniques to locate the coexistence density (*e.g.* using the Gibbs-ensemble method) fail. In our study, we have used a combination of non-Boltzmann sampling and histogram reweighting in both NPT-based and μVT-based ensembles. The details of the computational approach are described in the Appendix.

The very general nature of our model of DNA-coated particles with "long" DNA chains allows us to study the phase behavior a whole general class of systems. The specific details of each individual system (*e.g.*, salt concentration, *etc.*) could lead to small quantitative changes to the behavior of the system that can be added as further refinements to our model.

Results and discussion

Phase diagram

We studied a 1 : 1 binary mixture of our model system of DNA-coated particles using the non-Boltzmann-sampling MC methodology described in the Appendix. A complete set of simulations for a given model system yields the Helmholtz free energy (βA) of that system as a function of the total number of hybridize bonds (λ) and the logarithm of the volume ($\ln V$). One such free energy surface is presented in Fig. 1a for the case of a system with a valence (*i.e.*, number of DNA chains per particle) of $\kappa = 6$ and with a total of $\nu = 25$ colloids pairs (*i.e.*, a total of 50 colloids). From this free energy surface, coexistence can be determined at any given value of the hybridization free energy per bond (βf_{hyb}), by finding the pressure at which the probability histogram presents two peaks of equal area (see section on *Non-Boltzmann Sampling* in the Appendix). In Fig. 1b we present, for the same system, the probability histogram of visiting different values of $\ln V$ in the limit of $\beta f_{hyb} \to -\infty$ at coexistence conditions (*i.e.*, $P = 3.13 \times 10^{-6}$). The figure shows the existence of a bimodal probability distribution typical of first-order phase transitions. Moreover, since in the opposite limit [*i.e.*, $\beta f_{hyb} \to +\infty$ or $\Gamma = 0$, with $\Gamma \equiv \exp(-\beta f_{hyb})$] the particles behave simply as purely repulsive colloids with no first order phase transition, we can expect that in between these two limits there exists a critical value of βf_{hyb} below which the system phase separates. Thus, βf_{hyb} acts as the equivalent of the temperature in conventional liquid–vapor phase transitions.

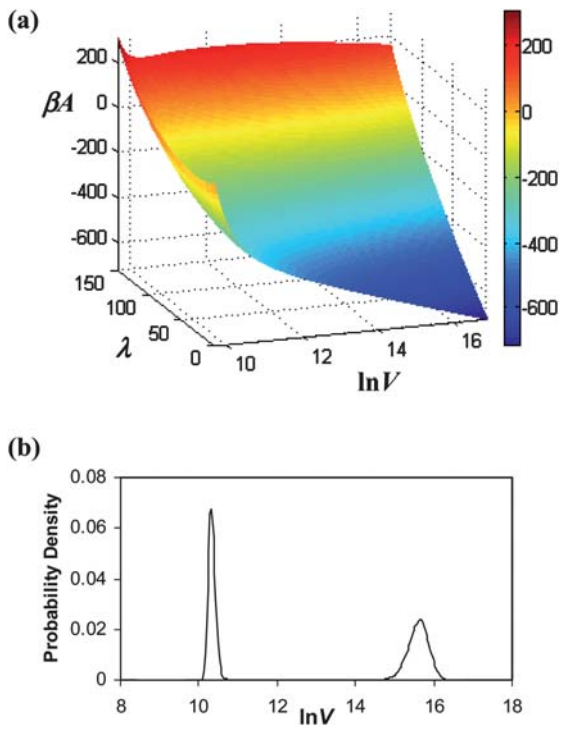

Fig. 1 Simulated system of a 1 : 1 mixture of 50 colloidal particles where each one of them has been coated with $\kappa = 6$ DNA chains. (a) Helmholtz free energy (βA) of the system as function of the macrovariables λ (*i.e.*, total number of bonds) and $\ln V$. (b) Probability histogram of visiting different values of $\ln V$ in the limit of $\Gamma \to \infty$. At coexistence conditions (*i.e.*, $P = 3.13 \times 10^{-6}$) the two peaks have equal area under the curve.

In Fig. 2, we present the coexistence phase diagram in the plane βf_{hyb} *vs.* the volume fraction of bare colloids (η) for the system with $\kappa = 6$. Below a certain value of βf_{hyb} the system undergoes macrophase separation into a dense liquid-like phase and a dilute vapor-like phase. Snapshots of these two phases in the strong hybridization limit (*i.e.*, $\Gamma \to \infty$) are shown in Fig. 3.

Good agreement was found for the phase diagrams obtained with the μVT- and NPT-type methods. The discrepancy between the two methods decreases with increasing system size. This is evident in the liquid branch of Fig. 2 where the results for the two "smaller" (S) systems differ the most while the results for the "larger" (L) systems are almost indistinguishable on the scale of figure. The NPT-L system had a total of $\nu = 25$ colloid pairs (*i.e.*, 50 colloids in total) while the NPT-S had $\nu = 15$. The μVT-L system had a simulation box edge size of $L_{box} = 37.5$ while the μVT-S had $L_{box} = 32$.

The coexistence envelope (binodal) is expected to end in a critical point. Indeed, for the case of $\kappa = 6$ we observe that the two distinct peaks of the density probability distribution merge into one at around $\beta f_{hyb} \approx -5$ thus setting an upper boundary for the critical value of βf_{hyb}. However, a more precise determination of the critical point would require a systematic finite-size scaling analysis.[47] This we have not attempted, as the precise values of

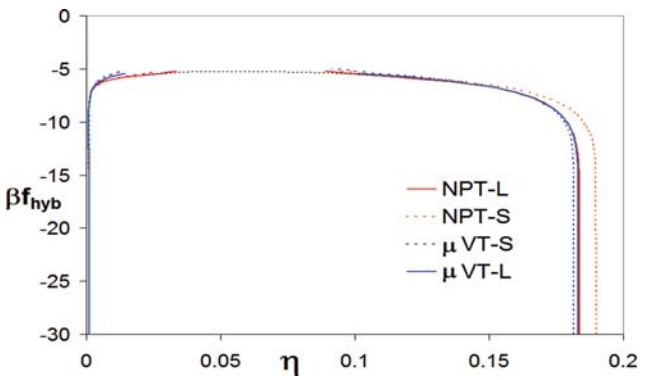

Fig. 2 Phase diagram for the system with $\kappa = 6$. The vertical axis represents the hybridization free energy (βf_{hyb}), the horizontal axis indicates the volume fraction of bare colloids (η). The parameter βf_{hyb} acts as the analog of temperature. Below a critical value (not shown) the system separates in liquid and vapor phases. The black dashed line around the critical region is just a guide for the eye. Results are shown for NPT-style and μVT-style simulations.

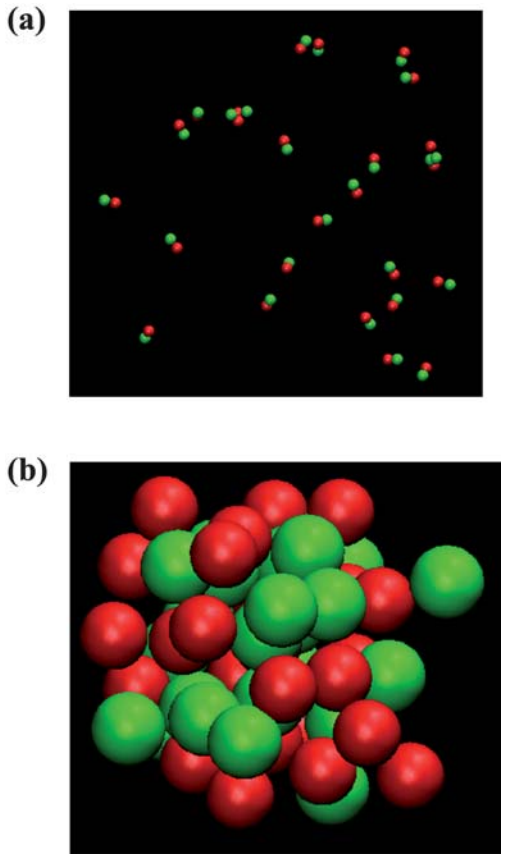

Fig. 3 Snapshots of the system with six DNA chains per particles in the in the limit of very negative βf_{hyb} (strong hybridization). (a) The vapor phase, mainly composed of A–B dimers. (b) The liquid phase. Different type colloids are represented with different colors (*i.e.*, red and green). For the sake of clarity, the DNA chains are not shown.

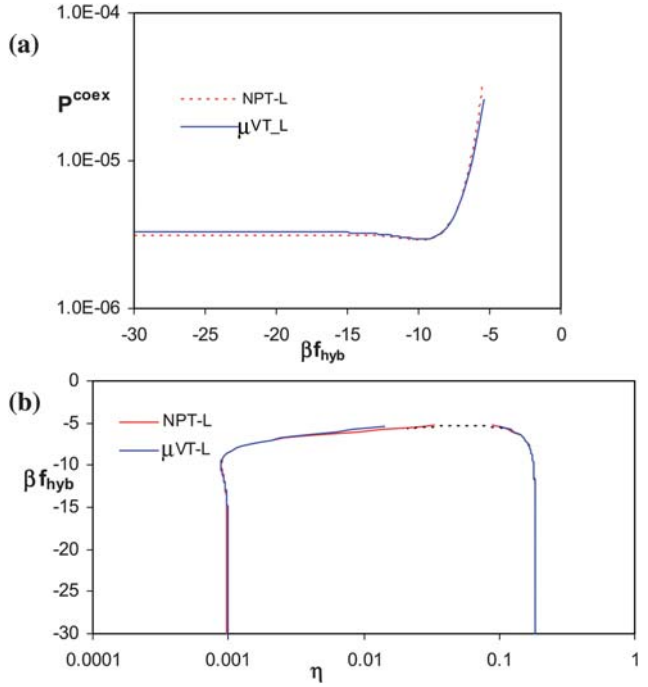

Fig. 4 Anomalous phase behavior of the DNA-coated particles systems. (a) It can be seen that the coexistence pressure (P^{coex}) is not a monotonic function of the equivalent temperature parameter βf_{hyb}. The value of P^{coex} exhibits a minimum around $\beta f_{hyb} = -9.8$. (b) The density of the coexistence vapor phase has a corresponding minimum at the same value of βf_{hyb}. The dashed line around the critical region is meant as guide for the eye.

the critical "temperatures" are of little relevance for the remainder of our analysis.

It is important to note that as the value of βf_{hyb} is decreased below -20 the coexistence densities are essentially the same as in the $\beta f_{hyb} \rightarrow -\infty$ limit for all the systems studied in this work.

Anomalous behavior

Fig. 4a shows the variation of the coexistence pressure (P^{coex}) with βf_{hyb} for the system with $\kappa = 6$. Interestingly, P^{coex} exhibits a minimum around the value of $\beta f_{hyb} = -9.8$. This contrast sharply with the monotonic temperature dependence of the vapor–liquid coexistence pressure that is normally observed along the boiling curve of atomic or molecular liquids. Similarly, Fig. 4b shows that, in a βf_{hyb} *vs.* η semi-log plot, the binodal also exhibits a density-minimum of the dilute phase at $\beta f_{hyb} = -9.8$.

In order to understand this anomaly it is helpful to examine the "Clausius–Clapeyron" equation for the dependence of the coexistence pressure on the hybridization free energy:

$$\frac{\partial P^{coex}}{\partial(\beta f_{hyb})} = -\frac{\lambda^v - \lambda^l}{V^v - V^l} \quad (5)$$

where the superscript v denotes the vapor (dilute) phase and the superscript l denotes the liquid (dense) phase. Since the volume of the vapor phase V^v is always larger than V^l eqn (5) indicates that at the value of $\beta f_{hyb} = -9.8$ the difference in number of bonds (*i.e.*, λ^v-λ^l) between the two phases changes sign. More specifically, for values of $\beta f_{hyb} > -9.8$ (*i.e.* at high temperatures), P^{coex} increases with βf_{hyb} because the liquid phase has a greater number of hybridized bonds than vapor phase, as one would intuitively assume. However, for values of $\beta f_{hyb} < -9.8$, this scenario inverts and (counter intuitively) the dilute phase becomes the one with the larger number of formed bonds.

It is instructive to plot the total hybridization free energy difference between the two phases [$\Delta\beta f_{hyb} = (\lambda^l - \lambda^v) \times \beta f_{hyb}$], normalized per colloid, as a function of βf_{hyb} (Fig. 5). For strongly negative values of βf_{hyb} both phases have essentially all the bonds satisfied and hence $\Delta\beta f_{hyb}$ is close to zero. Similarly, at the critical point (*i.e.*, $\beta f_{hyb} \approx -5$) both phases become identical and also $\Delta\beta f_{hyb} = 0$. Between these two extremes, we have a crossover in behavior where the system passes from a regime where it gains hybridization free energy upon condensation (*i.e.*, energy driven regime, $\beta f_{hyb} > -9.8$) to a regime where it **loses** hybridization free energy upon condensation (*i.e.*, entropy driven regime, $\beta f_{hyb} < -9.8$). In the former regime the system behaves as a classical liquid (*i.e.*, P^{coex} increases with "temperature") while in the latter regime the system presents anomalous behavior.

Fig. 5 provides an indication of the physical origin of the anomalous behavior. In this figure, a minimum of $\Delta\beta f_{hyb}$ is observed around $\beta f_{hyb} = -6.2$. If the difference λ^l-λ^v were constant, $\Delta\beta f_{hyb}$ would decrease linearly with βf_{hyb}. However, the presence of a minimum indicates that around $\beta f_{hyb} = -6.2$ the

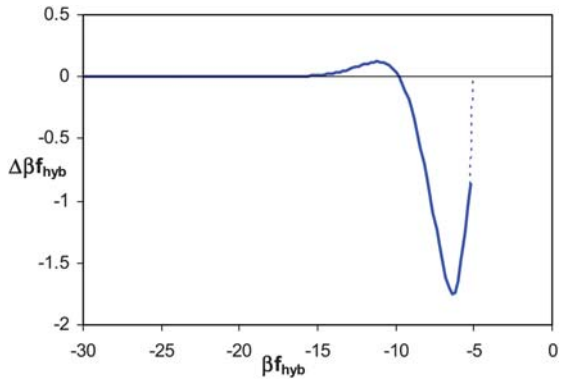

Fig. 5 Plot of the difference between the coexisting liquid and vapor phases of the total hybridization free energy [$\Delta\beta f_{hyb} = (\lambda^l - \lambda^v) \times \beta f_{hyb}$] per colloid, as a function of βf_{hyb}. The dashed curve is meant as a guide for the eye.

difference λ^l-λ^v changes much faster than βf_{hyb}, suggesting a dramatic transformation in the structure of the vapor phase.

In Fig. 6. we present plots of the probability f to find a colloid belonging to a cluster of a given size in the vapor phase. Fig. 6a shows f for the vapor phase at $\beta f_{hyb} = -10$ (*i.e.*, to the left of the minimum in $\Delta\beta f_{hyb}$), while Fig. 6b shows f at $\beta f_{hyb} = -5.8$ (*i.e.*, to the right of the minimum). At $\beta f_{hyb} = -10$ the vapor phase is predominantly composed of dimers, with some tetramers, and hexamers, but always in clusters composed of an even number of particles. However, at $\beta f_{hyb} = -5.8$, the system does not only contain even-numbered clusters, but also monomers and clusters containing an odd number of colloids. Since both types of colloids have the same valence ($\kappa = 6$), and each DNA chain can only bind to chains of the complementary type, the odd-numbered clusters will necessarily have "dangling bonds". Hence, in this regime the number of dangling bonds per colloid is less in the dense liquid phase where each colloid is surrounded by several neighbors. However, when $\beta f_{hyb} < -6.2$, the vapor phase contains mainly A–B dimers, virtually no monomers and a small number of other small even-numbered clusters. In this case, forming an additional bond in the vapor phase becomes facilitated as available complementary DNA chains can be found within a short distance. As a consequence, the number of bonds in the vapor phase increases faster than in the liquid phase as the hybridization strength is increased (βf_{hyb} made more negative). It is this effect that causes the change of sign of λ^l-λ^v at $\beta f_{hyb} = -9.8$. At this point, a new regime starts where the phase transition is dominated by the entropy of network formation. This entropy gain arises as the number of bond re-arrangements possible in a percolating-network liquid phase greatly exceeds the possibilities in a phase mainly formed by dimers.

In order to gain insight into the entropic nature of the phase transition it is convenient to compare our original system with a model system with exactly the same interactions but that can form dimers only. That is, once an individual "free" colloid makes a bond with another free colloid, it can form the rest of its bonds with its "partner" colloid only. Fig. 7 shows the difference (Δ) in the free energy βF, the configurational energy βU, the total hybridization free energy $\lambda \times \beta f_{hyb}$, and the negative of the entropy ($-S/k$) between the original system and the system that can form dimers only. These quantities are related through

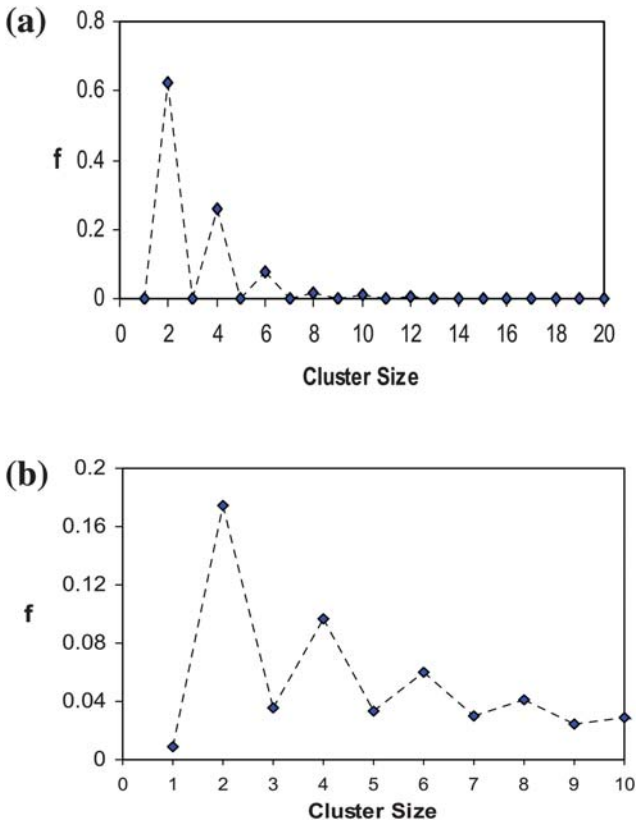

Fig. 6 Plots of the probability f to find a colloid belonging to a cluster of a given size in the vapor phase. (a) The vapor phase at $\beta f_{hyb} = -10$ (*i.e.*, to the left of the minimum in $\Delta\beta f_{hyb}$). All the clusters have an even number of colloids. (b) f at $\beta f_{hyb} = -5.8$ (*i.e.*, to the right of the minimum). Odd-numbered "frustrated" clusters are also present in the system.

$$\beta F = \beta U - \frac{S}{k} + \lambda \times \beta f_{hyb} \qquad (6)$$

All the quantities shown have been normalized by the number of colloid-pairs that are present in the system at any given point. When the system has only one pair of colloids, it can only form a dimer upon hybridization and $\Delta\beta F = 0$. However, as the number of colloid pairs (and the density) is increased, the original network-forming system becomes favored and $\Delta\beta F < 0$. Hence, explaining the transition to a percolated liquid at high densities.

In Fig. 7a we show the different components of the free energy in the limit of $\beta f_{hyb} \rightarrow -\infty$, where all the bonds are satisfied. Since in this limit both systems (*i.e.*, network-forming and dimers) have the same number of bonds, the difference in $\lambda \times \beta f_{hyb}$ is exactly zero, and therefore cannot be the driving force for the phase transition. On the other hand, both βU and $-S/k$ favor the network forming system. However, at liquid-like volume fractions (*i.e.*, $\eta > 0.1$), $-S/k$ clearly dominates over βU, illustrating the entropic nature of the phase transition. Actually, the term βU is not really energetic in nature as it derives from the coarse-grained representation of the interaction between athermal SAW chains. Therefore, βU is also entropic in nature: it represents the entropy associated with the overlapping and stretching of a SAW polymer. The value of $\Delta\beta U$ is negative because in a dimer the DNA chains need to migrate close to each other on the surface of

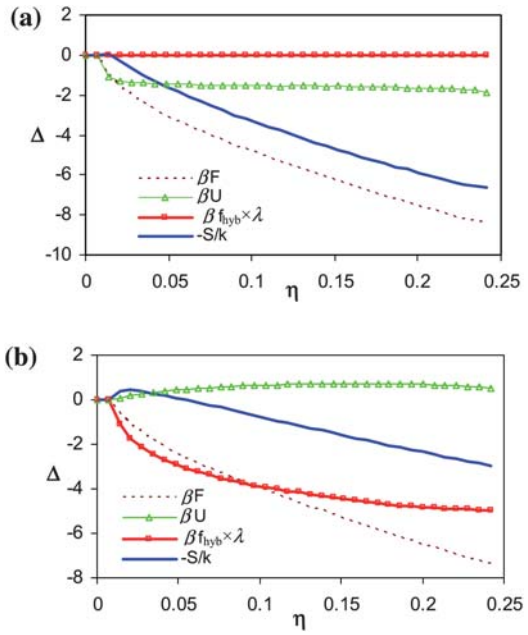

Fig. 7 Plot of the difference in free energy (βF) and its components [*i.e.*, configurational energy (βU), total hybridization free energy ($\lambda \times \beta f_{hyb}$), and negative of the entropy ($-S/k$)] between the original network-forming system and a reference system where only dimer formation is allowed. In the figure, the same symbol Δ is used to denote the difference in each of these four cases. The plots were obtained in μVT-type simulations where the density of the system was varied by adding/removing pairs (A–B) of colloids. (a) Limit of $\beta f_{hyb} \rightarrow -\infty$, the transition is driven by entropy. (b) $\beta f_{hyb} = -5.8$, the transition is driven by hybridization free energy.

the colloid in order to be able to form all the bonds, thereby increasing the repulsive interactions between blobs. Thus, while in this regime the phase transition is mainly driven by the entropy of bond-rearrangements, it is also favored by the gain in configurational entropy of the DNA chains implicitly taken into account *via* βU.

When $\beta f_{hyb} = -5.8$ (Fig. 7b) the free energy of the system still has some contributions from the entropy of bonds re-arrangements. However, its most important component now comes from the total hybridization free energy. Thus, in this regime the phase transition is hybridization-free-energy driven and therefore resembles the behavior of conventional liquid–vapor equilibria.

Finally, it is interesting to note that related anomalies to the ones observed in this work have been predicted for a fluid–fluid phase coexistence of metastable water. [45,46] Similar to the present case, the anomaly in the behavior of water has been related to an entropy driven phase transition wherein the system actually gains entropy upon reduction of its volume due to the breakage of hydrogen bonds.[45,46]

Effect of valence

Fig. 8 shows the phase diagram of DNA-coated particles with valence (κ) between 3 and 7. The phase diagram is shown in the $\eta - \beta f_{hyb}$ plane. It is readily observed that the binodal widens as κ increases. This behavior is to be expected as high-valence colloids gain more free energy upon condensation than low-valence colloids. As a consequence, the higher valence colloids have the lower coexistence pressure.

The phase behavior observed in our simulations can be compared with the experimental findings of Geerts *et al.*[13] who studied a system of DNA-coated colloids in the strong binding regime with a size ratio $R_g/R_c = 0.4$ (a size comparable to the one used in the present work, $R_g/R_c = 0.333$). In the experiments, the formation of large percolating clusters was observed. For the experimental system, the colloid volume fraction is known to be $\eta = 0.004$, but the number of DNA chains per colloid is only known approximately ($\kappa \approx 25$). Since our calculated binodal is expected to widen even more for $\kappa = 25$, our results suggest that the system studied in ref. 13 lies inside the coexistence region: the large percolating clusters observed in the experiments constitute the initial stages of the formation of the bulk of a liquid phase. However, as these clusters form, the bulk phase separation undergoes dynamical arrest.

As κ was lowered in our simulations, the difference between the densities of coexisting liquid and vapor phases decreased. Moreover, the minimum in the density probability distribution at coexistence between the "liquid" peak and the "vapor" peak becomes much less pronounced, which means that the free energy of the liquid–vapor interface decreases strongly (in particular, as the critical point is approached). Both factors make it more difficult to distinguish between the liquid and the vapor phase and this affects the reliability of the equal-area construction to determine coexistence. In addition, the coexistence properties of small-κ systems were found to have a pronounced system size dependence. Therefore, an accurate estimate of the binodal curve for $\kappa \leq 4$ would probably require a full finite-size scaling analysis,[47] something that goes beyond the scope of the present paper. In Fig. 8 we therefore only show that binodal up to βf_{hyb} values where our estimates are reliable. Beyond that, the drawn curves are only meant as a guide to the eye. In fact, the critical value of βf_{hyb} is not much larger (less negative) than the maximum value of βf_{hyb} for which the binodal could be determined reliably. The reason is that we found that even a slight increase in βf_{hyb} makes the surface tension go to zero. In addition, simulations on small systems tend to overestimate the temperature of the critical point. [47]

Finally, for the case $\kappa = 2$, we did not observe a bimodal density distribution for any of the system sizes studied. This suggests that the first-order liquid–vapor transition is suppressed. In fact, an

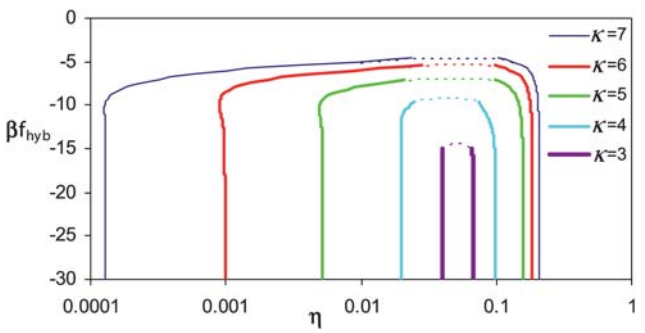

Fig. 8 Phase diagram of DNA-coated particles with valence (κ) between 3 and 7. Critical points are not shown. The dashed curves are meant as a guide for the eye. The labeling of the axes is as in Fig. 2.

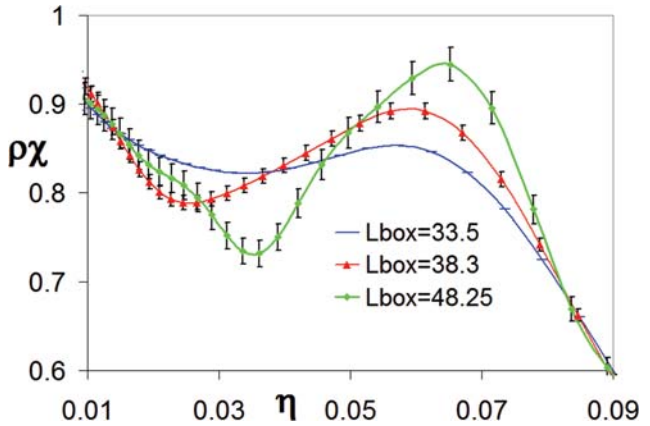

Fig. 9 The isothermal compressibility χ times the density ρ of the $\kappa = 2$ system in the infinitely-strong binding regime. The figure shows the progressive appearance of a peak (around $\eta \sim 0.065$) as the system size is increased, possibly suggesting a continuous phase transition.

analysis of a closely related lattice model[48] suggests that, indeed the $\kappa = 2$ has no phase transition at any finite value of βf_{hyb} – only in the low-temperature limit of infinitely negative hybridization free energies, the phase transition is expected to be an Ising-like continuous transition.[49] This qualitatively different behavior is not surprising as the $\kappa = 2$ system can only form one-dimensional clusters (*e.g.*, dimers, chains, rings, *etc.*). Evidence, for a possible continuous phase transition in the $\kappa = 2$ system, in the limit of infinitely negative hybridization free energy comes from the system-size dependence of the isothermal compressibility (χ) observed in Fig. 9. The figure shows the progressive appearance of a peak (around $\eta \sim 0.065$) as the system size is increased, suggesting a possible divergence of the compressibility in the thermodynamic limit.

Conclusions

In this paper we have used non-Boltzmann-sampling MC simulations together with histogram reweighting to study the phase behavior of a coarse grained representation of a binary system of colloids coated with long DNA strands. The system was observed to undergo phase separation into a dense liquid-like phase and a dilute vapor-like phase when the hybridization free energy (βf_{hyb}) was lowered below a certain critical value. Although in principle the value of βf_{hyb} can be made arbitrarily negative, we observed that for $\beta f_{hyb} < -20$ the system exhibited essentially the limiting $\beta f_{hyb} \rightarrow -\infty$ phase behavior.

The DNA-coated particles system exhibits a very unusual non-monotonic dependence of the coexistence pressure on βf_{hyb} (*i.e.*, the analog of the temperature), and displays a corresponding minimum in the coexistence vapor phase density. This anomalous behavior is understood in terms of a cross-over between entropy-driven regimes and hybridization-free-energy-driven regimes of the phase transition. We showed that the minimum in coexistence pressure marks the beginning of a regime where the vapor phase contains more hybridized bonds than the liquid phase, and that under these conditions the driving force for condensation is the increase in entropy due to bond re-arrangements in the dense network phase. Interestingly, similar anomalous behavior has been predicted for fluid-fluid phase transitions in water, where also an anticorrelation between entropy and volume is observed.[45,46]

We studied the effect of the number of DNA-chains per particle (κ) on the phase diagram. We found that the binodal widens with increasing κ, suggesting that the experiments of Geerts *et al.*,[13] with an estimated valence of $\kappa = 25$, were located inside the two-phase coexistence region.

For the case $\kappa = 2$, we did not find evidence of a first order phase transition at any value of βf_{hyb}. However, the dependence of the isothermal compressibility with system size in the infinite-binding-strength limit, suggests that a continuous phase transition may be present.

Appendix

In this Appendix we describe the simulation methodology used to locate the liquid–vapor coexistence curves of the model system under consideration.

Hybridization moves

In addition to the conventional MC moves required to equilibrate the system in a particular ensemble (*e.g.*, translations in the NVT ensemble, translations plus volume changes in the NPT ensemble, *etc.*)[50] the present system has the possibility of bond formation/destruction (*i.e.*, hybridization moves). The hybridization moves presented here are somewhat similar to those previously used in studies of quasi-block copolymers by Daoulas *et al.*[51] and other related systems.[52] However, in our particular system type-A blobs are only allowed to react with type-B blobs, and each blob can hybridize no more than once at a time. Then, the reaction moves (in the Canonical ensemble) are executed by first choosing with equal probability between bond formation and bond destruction. If bond formation is chosen, one randomly chooses one non-hybridized (free) A-blob and one free B-blob, and creates a bond with acceptance probability equal to

$$P_{acc} = \min\left[1, \frac{n_A \times n_B}{\lambda + 1} \times \exp\left(-\beta V_{har} - \beta f_{hyb}\right)\right] \qquad (7)$$

where $n_{A(B)}$ is the number of available A(B) reactive blobs, λ is the number of existing bonds, βV_{har} [*cf.* (4)] is the energy the new bond would have, and βf_{hyb} is the hybridization free energy per bond formed. Note that βf_{hyb} acts as an additive constant in βV_{har}, and determines the equilibrium concentration of bonds. Hence, βf_{hyb} is an intensive variable conjugate to the total number of bonds λ, that together with the specification of the variables NVT (for the case of the canonical ensemble) completely specifies the state of the system. Conversely, if bond destruction is chosen, one randomly chooses a bond and attempts to destroy it with probability

$$P_{acc} = \min\left[1, \frac{\lambda}{(n_A + 1) \times (n_B + 1)} \times \exp\left(\beta V_{har} + \beta f_{hyb}\right)\right] \qquad (8)$$

In practice, however, direct application of eqn (7) and (8) can be inefficient, as the probability of randomly choosing A and B blobs that are close enough for accepting the bond formation can be very low. Instead, it can be more convenient using a Rosenbluth-type bias[50] where bond creation is enacted by first randomly choosing an A-blob, and then, choosing a B-blob

among all the available B-blobs within a pre-specified cutoff distance from the A-blob, with probability proportional to

$$\sim \frac{\exp(-\beta V_{har})}{R_W} \tag{9}$$

where R_W is the Rosenbluth weight defined as

$$R_W = \sum \exp(-\beta V_{har}) \tag{10}$$

with the summation going over all the available B-blobs within cutoff distance. Finally, one accepts the move with probability

$$P_{acc} = \min\left[1, \frac{n_A \times R_W}{\lambda + 1} \times \Gamma\right] \tag{11}$$

where we have defined $\Gamma = \exp(-\beta f_{hyb})$. Similarly, after randomly choosing a bond, the bond-destruction moves are accepted with probability

$$P_{acc} = \min\left[1, \frac{\lambda}{(n_A + 1) \times R_W \times \Gamma}\right] \tag{12}$$

Here R_W is the Rosenbluth weight associated with the inverse (re-bonding) process. An important restriction in order to maintain detailed balance is that the bond to be destroyed has to have a length less than or equal to the cutoff distance, otherwise the move must be rejected.

The hybridization moves presented above, in addition to being valid for the canonical (ΓNVT) ensemble, are also valid for the isobaric-isothermic (ΓNPT) ensemble as long as the volume and the number of bonds are not changed simultaneously in the same move.

For the ΓNPT ensemble, we follow the formulation of Corti,[53] where the partition function is given by

$$Q_{\Gamma NPT} = \int_0^\infty Q_{\Gamma NVT} \times \exp[-\beta PV] d\ln V \tag{13}$$

where Q_i denotes the partition function of ensemble i. Hence, once a random change in $\ln V$ is proposed, one accepts with probability

$$P_{acc}(o \to n) = \min(1, \exp[-\beta \Delta U - \beta P \Delta V + N_p \ln(V_n/V_o)]) \tag{14}$$

where o stands for "old", n for "new", the symbol $\Delta Y = Y_n - Y_o$ for any variable Y, U is the configurational energy, N_p is the number of particles in the system whose coordinates has been re-scaled in the volume change process. During this move, the total number of bonds λ remains unchanged.

Non-boltzmann sampling

In principle one could determine the coexistence properties of the system during a ΓNPT simulation making use of the following recipe: (1) Guess a coexistence pressure (P^{coex}). (2) Make a histogram of how many times the system visits each value of $\ln V$. (3) Check that there are two peaks with equal area under the curve in the histogram. However, in practice, even if we knew the exact value of P^{coex}, the system would most likely remain trapped in only one of the two phases, therefore making the determination of the coexistence properties extremely difficult. Moreover, for large values of Γ, the probability of bond breakage will become vanishingly small [*cf.* eqn (12)], causing the system to become less ergodic as it can no longer easily explore the "bond-connectivity" space. Finally, we do not a priori know the value of P^{coex}, as this is one of the quantities we are after.

In order to overcome all the above difficulties, it is convenient to introduce arbitrary weights $\psi(\lambda, \ln V)$ that will enhance sampling (*e.g.*, multi-canonical sampling[54] or expanded ensemble[55]) over the complete range of allowed values of λ and $\ln V$. Since the volume is a continuous variable that can in principle go from zero to infinity it is convenient to discretize $\ln V$ (in this work we used $\Delta \ln V = 0.03$) and assign maximum and minimum values of $\ln V$ chosen so the system has a negligible probability of visiting them at the range of pressures of interest.

Thus, the acceptance rules designed for Boltzmann sampling in the previous section on "Hybridization Moves" have to be modified in order to incorporate the biasing weights ψ. Therefore we enact our hybridization moves for the Non-Boltzmann sampling (NBS) simulation[56] with acceptance probabilities

$$P_{acc} = \min\left[1, \frac{n_A \times R_W}{\lambda + 1} \times \exp\left[\psi_{\lambda+1, \ln V} - \psi_{\lambda, \ln V}\right]\right] \tag{15}$$

for bond creation, and

$$P_{acc} = \min\left[1, \frac{\lambda}{(n_A + 1) \times R_W} \times \exp\left[\psi_{\lambda-1, \ln V} - \psi_{\lambda, \ln V}\right]\right] \tag{16}$$

for bond destruction. Where the value of Γ (now irrelevant) has been set to $\Gamma = 1$ for convenience. Similarly, the volume moves (now between pre-specified discrete values of $\ln V$) are accepted with probability,

$$P_{acc}(o \to n) = \min(1, \exp[-\beta \Delta U + N_p \ln(V_n/V_o) + \psi_{\lambda, \ln Vn} - \psi_{\lambda, \ln Vo}]) \tag{17}$$

where again we set the (irrelevant) value of the pressure to $P = 0$.

It is straightforward to see that if we make the choice $\psi_{\lambda, lnV} = -\lambda \times \beta f_{hyb} - \beta PV$ we recover the Boltzmann-sampling rules. However, it is convenient to choose the ψ's in such way that the whole 2D space of $(\lambda, \ln V)$ allowed values is visited with equal frequency, though other choices can also be envisioned.[57–60]

Since the marginal probability (Π) of visiting a given "macrostate" (*i.e.*, a given point in the λ–lnV space) is given by

$$\Pi^{NBS}(\lambda, \ln V) \sim \Pi^{Boltz}(\lambda, \ln V) \exp[\psi_{\lambda, \ln V}] \tag{18}$$

To achieve uniform sampling we must choose

$$\psi_{\lambda, \ln V} = -\ln[\Pi^{Boltz}(\lambda, \ln V)] = -\ln[Q(\lambda, \ln V)] + C = \beta A(\lambda, \ln V) + C \tag{19}$$

where Q is the canonical partition function of a system with λ bonds and volume V, A is its free energy, and C is just an additive constant. Note that Q is **not** the partition function of a single system with a single "fixed" connectivity of bonds, but rather, it is a summation over all possible such systems, where the connectivity of the bonds have been re-arranged while keeping the total number of bonds equal to λ. In addition, since we are only concerned with differences in the weights ψ, the value of the constant C is irrelevant.

Although the values of $\beta A(\lambda, \ln V)$ are initially unknown, they can be estimated iteratively (up to a trivial constant) through

a variety of methods that include: using the histogram of visited states,[54,61] Wang–Landau sampling,[62] and, acceptance ratio methods[63–66] like the one proposed by Bennett.[67] In the present work we used Bennett's acceptance ratio method[67] to calculate free energy differences between neighboring macrostates, since it has been shown to utilize the data in an efficient way.[68] Bennett's acceptance ratio method has been used extensively in free energy calculations and details about its implementation can be found elsewhere.[66–69]

Since, the values of βA are independent of Γ and P, one can directly apply the histogram reweighting techniques[37,56] to obtain the $Q_{\Gamma NPT}$ (up to a multiplicative constant) at any value desired value of Γ and P through

$$Q_{\Gamma NPT} = \sum_{\ln V_{\min}}^{\ln V_{\max}} \left\{ \exp(-\beta PV) \sum_{\lambda=0}^{\lambda_{\max}} \exp\left[\lambda \ln\Gamma - \beta A(\lambda, \ln V) \right] \right\} \quad (20)$$

At a given value of Γ, the unnormalized probability distribution of the system being at a particular value of $\ln V$ is given by the quantity inside the curly brackets. Thus, in order to find P^{coex} one simply varies the value of the pressure until two equal area peaks are obtained in the probability distribution.

The histogram reweighting techniques described above have been widely used in the literature to study phase equilibria and a more detailed explanation about the method can be found elsewhere.[37,56,63,70]

Above, we have explained how to calculate phase coexistence in an NPT-like expanded ensemble, where we keep the number of particles constant and make changes in the volume. Equivalently, one can calculate phase coexistence in a μVT-like manner; that is, changing the number of particles while keeping the volume fixed.[70] Thus, one can envision an NBS scheme with the macrovariables being now λ, and the number of A–B colloid **pairs** ν. However, for DNA-coated particles there exists the additional complication that once bonds are formed, removing particles becomes highly impractical. For this reason, in the present work we only add/remove particles when no bonds are hybridized (*i.e.*, $\lambda = 0$). The hybridization moves are performed with acceptance rules analogous to those in (15) and (16). Insertions and deletions of colloid pairs are attempted with equal probabilities. The insertion of an A–B pair is accepted with probability:

$$P_{acc} = \min\left[1, \frac{V^2}{(N_A+1)\times(N_B+1)} \times \exp\left[-\beta\Delta U + \psi_{\lambda=0,\nu+1} - \psi_{\lambda=0,\nu}\right]\right] \quad (21)$$

while the deletion moves are accepted with

$$P_{acc} = \min\left[1, \frac{N_A \times N_B}{V^2} \times \exp\left[-\beta\Delta U + \psi_{\lambda=0,\nu-1} - \psi_{\lambda=0,\nu}\right]\right] \quad (22)$$

where $N_{A(B)}$ is the number of type-A(B) colloids already in the system and ΔU is the configurational energy change associated with the insertion/deletion process. In practice we use configurational bias to re-grow the DNA blobs.[50]

Again, we use Bennett's acceptance ratio method[67] to calculate the free energies [*i.e.*, $\beta A(\lambda,\nu)$] of each one of the macrostates. Finally, histogram reweighting can be used to find the partition function up to a multiplicative constant, $Q_{\Gamma\mu VT}$

$$Q_{\Gamma\mu VT} = \sum_{\nu=0}^{\nu_{\max}} \left\{ \exp(\nu\beta\mu^*) \sum_{\lambda=0}^{\lambda_{\max}(\nu)} \Gamma^{\lambda-\lambda_{\max}(\nu)} \exp\left[-\beta A(\lambda,\nu)\right] \right\} \quad (23)$$

where $\lambda_{\max}(\nu) = \kappa \times \nu$ is the maximum number of bonds for a given value of ν, and we have introduced for convenience $\beta\mu^* = \beta\mu + \kappa\ln\Gamma$, the chemical potential ($\beta\mu$) of non-bonded colloid pairs in a non-reactive ideal gas reservoir, shifted by the constant $\kappa\ln\Gamma$, with κ the number of DNA chains per colloid (*i.e.*, the valence of the colloid). Similarly, μ^* can be varied until the equal probability criterion is reached to find coexistence conditions, and the pressure can be obtained from the grand-partition function using the ideal gas state to determine the multiplicative constant[63,70] through,

$$\beta PV = \ln\left[\frac{Q_{\Gamma\mu VT} \times \exp(\beta A_{\lambda=0,\nu=0})}{2}\right] \quad (24)$$

Acknowledgements

This work was supported by the ERC (Advanced Grant agreement 227758). DF acknowledges support from a grant of the Royal Society of London (Wolfson Merit Award). We gratefully acknowledge CFN grant #528 that provided computer time on the Brookhaven CFN cluster. We thank Alexei Tkachenko for fruitful discussions.

References

1 C. A. Mirkin, R. L. Letsinger, R. C. Mucic and J. J. Storhoff, *Nature*, 1996, **382**(6592), 607–609.
2 R. C. Mucic, J. J. Storhoff, C. A. Mirkin and R. L. Letsinger, *J. Am. Chem. Soc.*, 1998, **120**(48), 12674–12675.
3 A. P. Alivisatos, K. P. Johnsson, X. G. Peng, T. E. Wilson, C. J. Loweth, M. P. Bruchez and P. G. Schultz, *Nature*, 1996, **382**(6592), 609–611.
4 T. Schmatko, B. Bozorgui, N. Geerts, D. Frenkel, E. Eiser and W. C. K. Poon, *Soft Matter*, 2007, **3**(6), 703–706.
5 H. D. Hill, S. J. Hurst and C. A. Mirkin, *Nano Lett.*, 2009, **9**(3), 1283–1283.
6 A. J. Kim, P. L. Biancaniello and J. C. Crocker, *Langmuir*, 2006, **22**, 1991–2001.
7 S. Y. Park, A. K. R. Lytton-Jean, B. Lee, S. Weigand, G. C. Schatz and C. A. Mirkin, *Nature*, 2008, **451**(7178), 553–556.
8 R. J. Macfarlane, B. Lee, H. D. Hill, A. J. Senesi, S. Seifert and C. A. Mirkin, *Proc. Natl. Acad. Sci. U. S. A.*, 2009, **106**(26), 10493–10498.
9 D. Nykypanchuk, M. M. Maye, D. van der Lelie and O. Gang, *Nature*, 2008, **451**(7178), 549–552.
10 H. M. Xiong, D. van der Lelie and O. Gang, *J. Am. Chem. Soc.*, 2008, **130**(8), 2442–2443.
11 H. M. Xiong, D. van der Lelie and O. Gang, *Phys. Rev. Lett.*, 2009, **102**(1), 015504.
12 M. M. Maye, M. T. Kumara, D. Nykypanchuk, W. B. Sherman and O. Gang, *Nat. Nanotechnol.*, 2010, **5**(2), 116–120.
13 N. Geerts, T. Schmatko and E. Eiser, *Langmuir*, 2008, **24**(9), 5118–5123.
14 A. V. Tkachenko, *Phys. Rev. Lett.*, 2002, **89**(14), 148303.
15 M. E. Leunissen, R. Dreyfus, R. J. Sha, T. Wang, N. C. Seeman, D. J. Pine and P. M. Chaikin, *Soft Matter*, 2009, **5**(12), 2422–2430.
16 M. E. Leunissen, H. R. Vutukuri and A. van Blaaderen, *Adv. Mater.*, 2009, **21**(30), 3116.
17 M. E. Leunissen, R. Dreyfus, F. C. Cheong, D. G. Grier, R. Sha, N. C. Seeman and P. M. Chaikin, *Nat. Mater.*, 2009, **8**(7), 590–595.

18 R. Dreyfus, M. E. Leunissen, R. J. Sha, A. V. Tkachenko, N. C. Seeman, D. J. Pine and P. M. Chaikin, *Phys. Rev. Lett.*, 2009, **102**(4), 048301.
19 M. E. Leunissen, R. Dreyfus, R. Sha, N. C. Seeman and P. M. Chaikin, *J. Am. Chem. Soc.*, 2010, **132**(6), 1903–1913.
20 A. J. Kim, R. Scarlett, P. L. Biancaniello, T. Sinno and J. C. Crocker, *Nat. Mater.*, 2009, **8**(1), 52–55.
21 C. W. Hsu, J. Largo, F. Sciortino and F. W. Starr, *Proc. Natl. Acad. Sci. U. S. A.*, 2008, **105**(37), 13711–13715.
22 W. Dai, C. W. Hsu, F. Sciortino and F. W. Starr, *Langmuir*, 2010, **26**(5), 3601–3608.
23 B. D. Rabideau and R. T. Bonnecaze, *Langmuir*, 2007, **23**(20), 10000–10007.
24 O. S. Lee and G. C. Schatz, *J. Phys. Chem. C*, 2009, **113**(6), 2316–2321.
25 T. E. Ouldridge, I. G. Johnston, A. A. Louis and J. P. K. Doye, *J. Chem. Phys.*, 2009, **130**, 065101.
26 P. D. Dans; A. Zeida; M. a. R. Machado,; S. Pantano, *Journal of Chemical Theory and Computation*.
27 M. W. Matsen, *J. Phys.: Condens. Matter*, 2002, **14**(2), R21–R47.
28 F. J. Martinez-Veracoechea and F. A. Escobedo, *Macromolecules*, 2009, **42**(22), 9058–9062.
29 F. J. Martinez-Veracoechea and F. A. Escobedo, *Macromolecules*, 2009, **42**(5), 1775–1784.
30 N. Osterman, I. Poberaj, J. Dobnikar, D. Frenkel, P. Ziherl and D. Babic, *Phys. Rev. Lett.*, 2009, **103**(22), 228301.
31 C. N. Likos, B. M. Mladek, A. J. Moreno, D. Gottwald and G. Kahl, *Comput. Phys. Commun.*, 2008, **179**(1–3), 71–76.
32 I. Coluzza and J. P. Hansen, *Phys. Rev. Lett.*, 2008, **100**(1), 016104.
33 B. Bozorgui and D. Frenkel, *Phys. Rev. Lett.*, 2008, **101**(4), 045701.
34 A. Zilman, J. Kieffer, F. Molino, G. Porte and S. A. Safran, *Phys. Rev. Lett.*, 2003, **91**(1), 015901.
35 A. Zilman, T. Tlusty and S. A. Safran, *J. Phys.: Condens. Matter*, 2003, **15**(1), S57–S64.
36 A. Z. Panagiotopoulos, N. Quirke, M. Stapleton and D. J. Tildesley, *Mol. Phys.*, 1988, **63**(4), 527–545.
37 A. M. Ferrenberg and R. H. Swendsen, *Phys. Rev. Lett.*, 1988, **61**(23), 2635–2638.
38 A. Z. Panagiotopoulos, *J. Phys.: Condens. Matter*, 2000, **12**(3), R25–R52.
39 A. A. Louis, P. G. Bolhuis, J. P. Hansen and E. J. Meijer, *Phys. Rev. Lett.*, 2000, **85**(12), 2522–2525.
40 A. Pelissetto and J. P. Hansen, *J. Chem. Phys.*, 2005, **122**(13), 134904.
41 C. Pierleoni, B. Capone and J. P. Hansen, *J. Chem. Phys.*, 2007, **127**(17), 171102.
42 A. Pelissetto and J. P. Hansen, *Macromolecules*, 2006, **39**(26), 9571–9580.
43 B. v. Lengerich, R. J. Rawle, and S. G. Boxer, *Langmuir*, 2010, **26**, 8666.
44 S. J. Stranick, A. N. Parikh, D. L. Allara and P. S. Weiss, *J. Phys. Chem.*, 1994, **98**(43), 11136–11142.
45 G. Franzese and H. E. Stanley, *J. Phys.: Condens. Matter*, 2002, **14**(9), 2201–2209.
46 K. Stokely, M. G. Mazza, H. E. Stanley and G. Franzese, *Proc. Natl. Acad. Sci. U. S. A.*, 2010, **107**(4), 1301–1306.
47 K. Binder, *Eur. Phys. J. B*, 2008, **64**(3–4), 307–314.
48 E. Domany, D. Mukamel, B. Nienhuis and A. Schwimmer, *Nucl. Phys. B*, 1981, **190**(2), 279–287.
49 We thank B. Nienhuis for bringing ref. 48 to our attention.
50 D. Frenkel; B. Smit., *Understanding Molecular Simulation*. Academic Press: San Diego, CA, 2002.
51 K. C. Daoulas, A. Cavallo, R. Shenhar and M. Muller, *Soft Matter*, 2009, **5**(22), 4499–4509.
52 C. C. Huang; H. Xu; F. Crevel; J. Wittmer; J. P. Ryckaert. *Computer Simulations in Condensed Matter Systems: From Materials to Chemical Biology, Vol 2* 2006, 704, pp. 379–418.
53 D. S. Corti, *Mol. Phys.*, 2002, **100**(12), 1887–1904.
54 B. A. Berg and T. Neuhaus, *Phys. Rev. Lett.*, 1992, **68**(1), 9–12.
55 A. P. Lyubartsev, A. A. Martsinovski, S. V. Shevkunov and P. N. Vorontsovvelyaminov, *J. Chem. Phys.*, 1992, **96**(3), 1776–1783.
56 C. R. A. Abreu and F. A. Escobedo, *J. Chem. Phys.*, 2006, **124**(5), 054116.
57 S. Trebst, D. A. Huse and M. Troyer, *Phys. Rev. E: Stat., Nonlinear, Soft Matter Phys.*, 2004, **70**(4), 046701.
58 F. A. Escobedo and F. J. Martinez-Veracoechea, *J. Chem. Phys.*, 2008, **129**(15), 154107.
59 F. J. Martinez-Veracoechea and F. A. Escobedo, *J. Phys. Chem. B*, 2008, **112**(27), 8120–8128.
60 C. R. A. Abreu, *J. Chem. Phys.*, 2009, **131**, 154113.
61 I. Coluzza and D. Frenkel, *ChemPhysChem*, 2005, **6**(9), 1779–1783.
62 F. G. Wang and D. P. Landau, *Phys. Rev. Lett.*, 2001, **86**(10), 2050–2053.
63 J. R. Errington and A. Z. Panagiotopoulos, *J. Chem. Phys.*, 1998, **109**(3), 1093–1100.
64 J. K. Singh and J. R. Errington, *J. Phys. Chem. B*, 2006, **110**(3), 1369–1376.
65 M. S. Shell, P. G. Debenedetti and A. Z. Panagiotopoulos, *J. Chem. Phys.*, 2003, **119**(18), 9406–9411.
66 F. A. Escobedo and C. R. A. Abreu, *J. Chem. Phys.*, 2006, **124**(10), 104110.
67 C. H. Bennett, *J. Comput. Phys.*, 1976, **22**(2), 245–268.
68 M. K. Fenwick and F. A. Escobedo, *J. Chem. Phys.*, 2004, **120**(7), 3066–3074.
69 I. D. Gospodinov and F. A. Escobedo, *J. Chem. Phys.*, 2005, **122**(16), 164103.
70 J. R. Errington, *J. Chem. Phys.*, 2003, **118**(22), 9915–9925.